Calculation of Shock Waves and Temperatures of FCC Single Crystals (Nickel) using Large-Scale Molecular Dynamics

Oyeon Kum
Department of Chemistry, Clemson University, Clemson, SC 29634, USA
okum@clemson.edu

ABSTRACT

Multimillion-atom (two to four million atoms) molecular dynamics simulations using double-SPMD (SPSPMD: scalable parallel soft potentials molecular dynamics) code have been applied to calculate fcc single crystal, nickel, shock wave and temperature profiles on a CrayT3E. Three well known model potentials, analytical embedded-atom method (EAM) potential, Morse potential, and Voter's data table EAM potential were used for fcc single crystal nickel. Orientation dependent effects on shock propagation profiles, shock tip movements, and temperature profiles were observed. Orientation dependent effects on shock wave propagation showed anisotropy of the fcc single crystals along the different shock propagation directions. Shock tip movement profiles for Morse potential and data EAM potential showed similar patterns in all orientations. Temperature profiles also showed anisotropy, corresponding to pressure profiles, in different orientations.

Keywords: double-SPMD, shock wave and temperature profiles, fcc single crystal, anisotropy

1 INTRODUCTION

The planar shock waves in a dense medium exhibit a sharp rise in density, velocity, pressure, and energy with widths as little as a couple of mean atomic spacings (nearest neighbor distances in solids and dense liquids are typically of the order of 0.3 nm) [1]. The rising time of the shock waves is as short as a vibrational period in the solid (or mean collision time in the fluid), which is of the order of 0.3 ps [1]. These extremely tiny time and distance scales make the large scale MD simulations the most successful tool for studying the collective motion of large numbers of atoms engaged in nonequilibrium flows. Historically, near the beginning of the 1970's, William G. Hoover pioneered the method of nonequilibrium molecular dynamics (NEMD) [2, 3]. NEMD applies experimental driving forces and constraints, similar to those imposed in the laboratory, but at the atomic scale, in order to induce nonequilibrium steady-state flows of mass and energy. Though NEMD and shock waves are ideally coupled, the samples subjected to shock waves in NEMD must be sufficiently long to get planar steady waves, which are studied in laboratory experiments using gas guns. They become steady in time by virtue of the transport of energy and momentum from the direction of propagation into transverse dimensions. Hence, the transverse dimension of the sample must be large enough to get realistic viscous damping in fluids, or reversible elastic torsion and irreversible plastic flow in solids. Therefore, only multimillion-atom MD simulations are suited to get realistic dissipation mechanism and steady planar shock waves. Even the state of the art computer technology can not handle such a big system on a single processor. The double-SPMD code whose parallel algorithm was derived from the parallel smooth particle applied mechanics (SPAM) code [4] was used for this study.

In this paper, three soft potentials for fcc single crystals of nickel were used: a Morse pair potential with spline tail (MORSE), an analytical EAM (A-EAM) potential, and Voter's data-table EAM potential (D-EAM) [5]. The shock waves and corresponding temperatures were calculated in three different crystallographic orientations to study orientation effects of shocked single crystals. Though all calculations were done on the CrayT3E supercomputer with 50 PEs at the Korea Institute of Science and Technology Information in Korea, this code is portable to any computer with MPI message passing interface. Recently, this code was modified to run on a small Beowulf PC Cluster with the Linux operating system and MPI message passing interface, developed by the author at the Institute for Shock Physics, Washington State University [6].

2 SIMULATION MODEL AND METHOD

Double-SPMD code is a three dimensional parallel MD code with 4th-order Runge-Kutta integration algorithm and periodic boundary conditions. The domain decomposition algorithm is identical to that of the author's smooth particle applied mechanics (SPAM) code for fluid dynamics studies [4]. The computational region is divided into a large number of cells which are assigned to PEs. Particles are assigned to processors geometrically according to their coordinates. For a large set of particles, the region assigned to each processor will have dimensions significantly larger than the interaction cut-off distance, r_{max}. In general, there will be a large number of particles on each processor that do not interact with each other. The region on each processor is subdivided into large collection of smaller cells whose size is still larger than the interaction cut-off. All processors have the same number of cells to ensure proper load balancing. This cell structure of the algorithm forms coarse-grained multi-

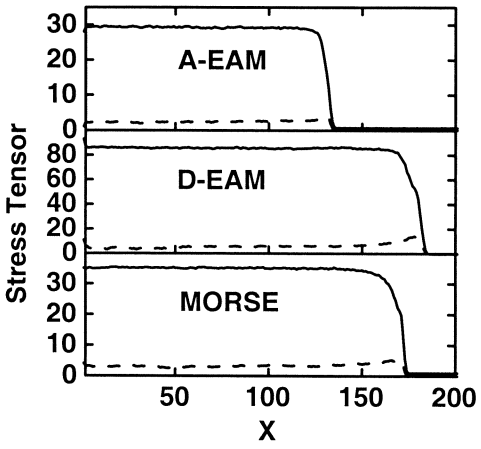

Figure 1: Left half profiles of longitudinal component of the pressure-volume tensor $P_{xx}V$ (solid curve) and twice the shear component $[P_{xx} - \frac{1}{2}(P_{yy} + P_{zz})]V$ (dashed curve) in $\langle 100 \rangle$ shocks at time about 3.8 psec for A-EAM and MORSE and 4.8 psec for D-EAM. Horizontal axis X represents the number of crystal planes in the longitudinal direction. The stress tensor is given in reduced units for A-EAM and MORSE, but GPa unit for D-EAM. Piston velocity is about 1.5 Km/sec, above the critical shock strength. From top to bottom, analytical-EAM potential (A-EAM), data table EAM potential (D-EAM), and MORSE potential with spline tail (MORSE), respectively.

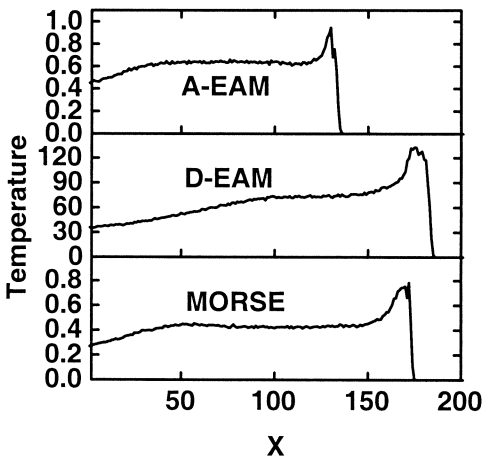

Figure 2: Left half temperature profiles in $\langle 100 \rangle$ shocks. Unit of temperature is degree Kelvin (K) for D-EAM but reduced units for A-EAM and MORSE. (see figure 1 for keys and details).

cell method.

In this study, different lengths of long parallelepiped in the direction of shock propagation were used depending on the potential models and the crystallographic orientations: in the $\langle 100 \rangle$ direction, 400 fcc lattice planes with 5000 atoms in each plane were stacked as an ABAB $\cdots$ pattern for a total of 2 000 000 atoms for all three potentials; in the $\langle 110 \rangle$ orientation, 1140, 1140, and 1000 fcc lattice planes with 3 500, 3 500, and 3 550 atoms were used in each plane as an ABAB $\cdots$ pattern for a total of 3 990 000, 3 990 000, and 3 550 000 atoms for the MORSE, A-EAM, and D-EAM potentials, respectively; in the $\langle 111 \rangle$ shocks, 600, 600, and 690 lattice planes with 5 904, 5 904, and 5 520 atoms were used in each plane as an ABCABC $\cdots$ pattern for a total of 3 542 400, 3 542 400, and 3 808 800 atoms for the MORSE, A-EAM, and D-EAM potentials, respectively. The cross-sectional plane in all potentials and orientations corresponds to 50 $\sim$ 53 by 50 $\sim$ 53 fcc unit cells. The longitudinal dimension, converted to the physical units appropriate for nickel, corresponds to about 0.3 μm.

3 RESULTS AND DISCUSSIONS

Figure 1 shows the left half profiles of longitudinal and shear stresses for steady state shock waves traveling in the $\langle 100 \rangle$ direction for the analytical EAM, data-table EAM, and Morse potentials, respectively. The piston speed, u_p, is about 1.5 km/sec, greater than critical shock strength, $0.2c_l$, about 1.0 km/sec for nickel, where c_l is the longitudinal sound velocity. Strong plastic waves almost overtook the elastic precursors (almost complete shear-stress relaxation) but the emergence of an unsteady elastic precursor followed by the steady plastic wave is still seen for all three potentials. The shock tip profile of D-EAM is almost the same as those of MORSE. However, the shock wave speeds of both EAM potentials are slower than that of MORSE.

Figure 2 shows the temperature profiles corresponding to Figure 1. Temperature increases sharply at the shock tip area which is considered to be the leading force of shock waves. In the middle region, corresponding to equilibrium region, the temperature is constant. However, near the piston area, the temperature decreases due to shock wave relaxations in $\langle 100 \rangle$ shocks. The relaxation length is different for different potentials and is known to depend, somewhat, on the boundary conditions. The maximum temperature is about 120 K for these shocks. The relaxation pattern (near piston region) of A-EAM is similar to that of MORSE but different from that of D-EAM. D-EAM has longer range than the others.

The profiles in Figure 3 show steady state longitudinal and shear stresses traveling along the $\langle 110 \rangle$ direction with the same piston speed as in Figure 1. But completely new behavior can be seen in this orientation. Three distinct regimes are seen: a leading solitary wave train followed by an extended precursor and finally by a plastically deformed region. Each soliton pulse is well stabilized and a compressive zone roughly three-lattice-planes-wide appears with atoms compressed primarily along longitudinal direction but very little, if at all, along the transverse directions. The stability of the

solitary wave train depends on the temperature and the defects in real crystals. It was observed that solitary waves remained stable up to $T_o \simeq T_{melt}/10$, whereas such nonsteady wave trains were seen only along the ⟨100⟩ direction if the initial temperature is zero [7]. Though the stabilized solitary wave trains are seen for both EAM and pair potentials, EAM has smaller number of solitons, and behaves much like a high temperature model.

The profiles in the Figure 4 show the temperature profiles corresponding to Figure 3. In the shock tip areas, the profile looks much like that of pressure with solitons. In the elastic region just behind the shock tip area, the temperature decreases. However, in the middle of equilibrium region, temperature increases very sharply to reach the maximum near the piston boundary. The decreasing shapes from hot area to cold area are different for different potentials, which helps to explain the relaxation characteristics of the given potential functions.

The profiles of longitudinal and shear stress waves in ⟨111⟩ shocks are seen in Figure 5. In this figure, the piston velocity for D-EAM is about 1.7 Km/sec, higher than the other directions. For piston velocities sufficient to initiate plastic deformation (shown by the relaxation of shear stress behind the shock front), a long and unsteady elastic shock front leads the steady plastic wave. This elastic precursor region was not seen in Figure 1, in the ⟨100⟩ orientation. There is large difference in the length of the elastic precursor region between A-EAM and both MORSE and D-EAM. However, it looks similar for both MORSE and D-EAM. Some solitary waves in MORSE and D-EAM were observed. These solitary wave trains remind us of the old problem that the more conventional continuum approach may not be suitable for adequately describing the shock profiles in solids because a discrete lattice exhibits a dispersion which is not accounted for in the usual continuum approaches.

Figure 6 shows the corresponding temperature profiles. In the shock tip area and just behind elastic area, the temperature profiles look similar to those of stresses. In the middle of the equilibrium region, it shows the same decreasing profiles as those of ⟨110⟩ shocks. However, the maximum increase occurred far from of the piston boundary, similar to those of ⟨100⟩ shocks, compared to those of ⟨110⟩ orientation.

4 CONCLUSIONS

Systematic large-scale molecular dynamics simulations were carried out for fcc single crystals which were described by three potentials using double-SPMD. Orientation dependent effects on shock propagation in a single crystal showed both the anisotropy of the crystal and the dispersion of the discrete lattice that are not well accounted for in the usual continuum approach, as described in the other large-scale simulation in reference [7]. The three potentials showed similar behavior for shock wave propagation and temperature profiles of FCC single crystals as a whole: solitary wave train in ⟨110⟩ orientation and inclined and declined temperature

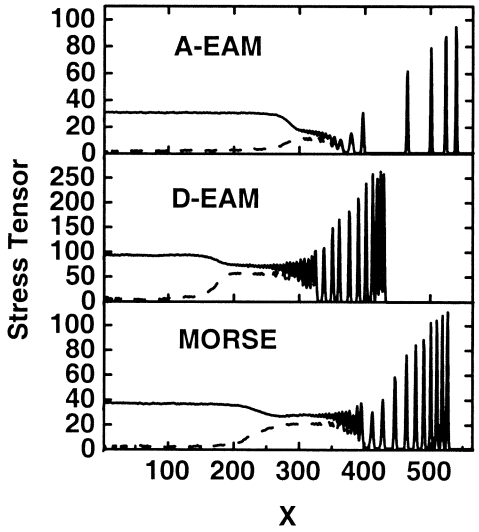

Figure 3: Left half profiles of longitudinal component of the pressure-volume tensor (solid curve) and twice the shear component (dashed curve) in ⟨110⟩ shocks at time about 6.4, 5.1, and 5.3 psec for A-EAM, D-EAM, and MORSE, respectively. (see figure 1 for keys and details).

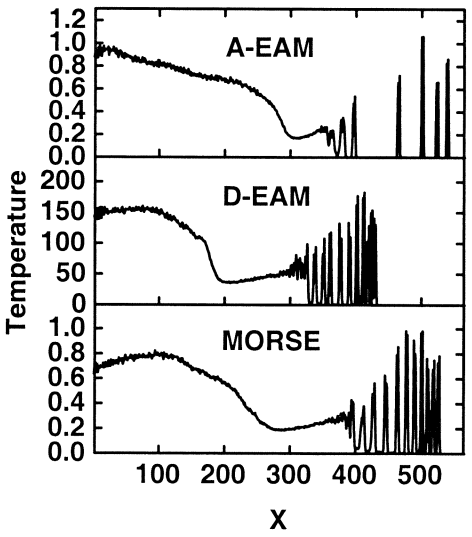

Figure 4: Left half temperature profiles in ⟨110⟩ shocks. (see figure 1 and figure 2 for keys and details).

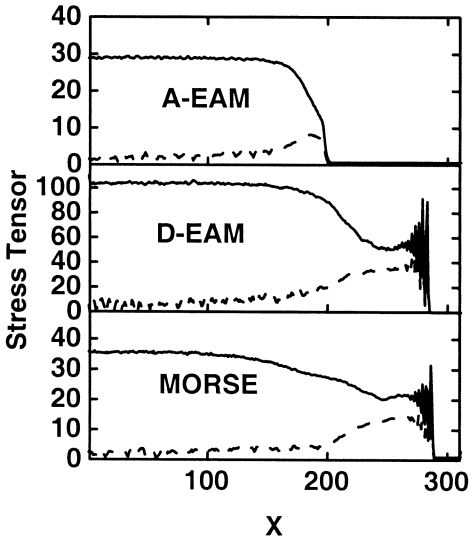

Figure 5: Left half profiles of longitudinal component of the pressure-volume tensor (solid curve) and twice the shear component (dashed curve) in ⟨111⟩ shocks at time about 6.0, 6.9, and 6.0 psec for A-EAM, D-EAM, and MORSE, respectively. The piston velocities are about 1.5 Km/sec for A-EAM and MORSE, and 1.7 Km/sec for D-EAM. (see figure 1 for keys and details).

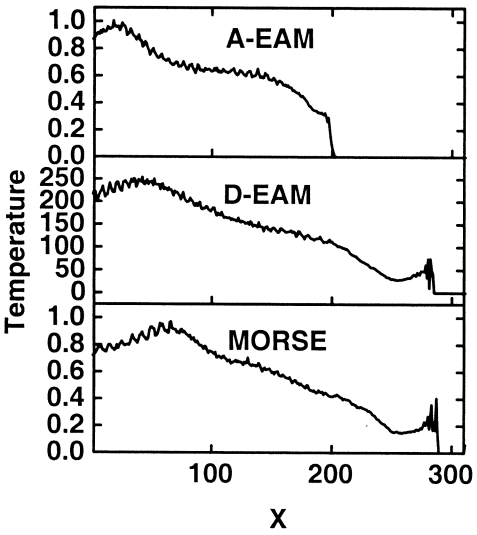

Figure 6: Left half temperature profiles in ⟨111⟩ shocks. (see figure 1 and figure 2 for keys and details).

profiles in all directions. However, the shock wave propagation speeds for the two EAM potentials were a bit slower than that of the Morse potential. These differences could be expected from the fact that the EAM potential does not satisfy the Cauchy relation while pair potentials do at very low temperature, though it is also violated slightly by thermal effects even with pair potentials. More interesting result shown in this study is that shock waves and temperatures for D-EAM are very similar to those of MORSE, rather than A-EAM.

ACKNOWLEDGMENTS

Yo-Han Yoo is thanked for generous allowance of the computer account. Brad Holian and Timothy Germann are thanked for useful comments and advices. Arthur Voter is thanked for providing his data table EAM potentials and many useful comments about the potentials. Steve Stuart and Brad Dickson are thanked for their proofreadings and many useful comments.

References

[1] B.L. Holian, unfinished manuscript for shock waves and condensed matter conference, 2001.

[2] W.G. Hoover, Structure of a Shock-Wave Front in a Liquid, *Phys. Rev. Lett.* **42 (23)**, 1531-1534, 1979.

[3] J. H. Batteh and J. D. Powell, Shock propagation in the one-dimensional lattice at a nonzero initial temperature, *J. Appl. Phys.* **49 (7)**, 3933-3940, 1978.

[4] O. Kum, K. Hahn, S. Kim, and J. Kwon, "High Performance Computing on the Information Superhighway, April 28 - May 2, 1977 Seoul Korea ", IEEE Computer Society Press, 661-666, 1997.

[5] A.F. Voter, *Embedded Atom Method Potentials for Seven FCC metals: Ni, Pd, Pt, Cu, Ag, Au, and Al*, Los Alamos Unclassified Technical Report #LA-UR 93-3901, 1993.

[6] O. Kum and Y.M. Gupta, manuscript prepared for Journal of Applied Physics, 2002; O. Kum, "Beowulf PC Cluster", manuscript for the Institute for Shock Physics, Washington State University, October, 2001.

[7] T.C. Germann, B.L. Holian, and P.S. Lomdahl, Orientation Dependence in Molecular Dynamics Simulation of Shocked Single Crystals, *Phys. Rev. Lett.* **84 (23)**, 5351-5354, 2000.